High-resolution X-ray fluorescence-based provenance mapping of Eocene fluvial distributary fans that fed ancient Gosiute Lake, Wyoming, USA

M.E. Smith[1,†], H.G. Gregorich[1], L.A. Gipson[1], R.C. Krueger[1], A.R. Carroll[2], E.C. Parrish[2], A.P. Walters[3], S. Honig[2], C. Schwaderer[2], S. Meyers[2], B.S. Singer[2], T.K. Lowenstein[4], and W.D. Arnuk[4]

[1]*School of Earth and Sustainability, Northern Arizona University, 624 South Knoles Drive, Flagstaff, Arizona 86011, USA*
[2]*Department of Geoscience, University of Wisconsin–Madison, 1215 West Dayton Street, Madison, Wisconsin 53706, USA*
[3]*Department of Geology, Cornell College, 600 First Street SW, Mount Vernon, Iowa 52314, USA*
[4]*Department of Earth Sciences, Binghamton University, 4400 Vestal Parkway East, Binghamton, New York 13902, USA*

ABSTRACT

The Green River Formation of Wyoming, USA, is host to the world's largest known lacustrine sodium carbonate deposits, which accumulated in a closed basin during the early Eocene greenhouse. Alkaline brines are hypothesized to have been delivered to ancient Gosiute Lake by the Aspen paleoriver that flowed from the Colorado Mineral Belt. To precisely trace fluvial provenance in the resulting deposits, we conducted X-ray fluorescence analyses and petrographic studies across a suite of well-dated sandstone marker beds of the Wilkins Peak Member of the Green River Formation. Principal component analysis reveals strong correlation among elemental abundances, grain composition, and sedimentary lithofacies. To isolate a detrital signal, elements least affected by authigenic minerals, weathering, and other processes were included in a principal component analysis, the results of which are consistent with petrographic sandstone modes and detrital zircon chronofacies of the basin. Sandstone marker beds formed during eccentricity-paced lacustrine lowstands and record the migration of fluvial distributary channel networks from multiple catchments around a migrating depocenter, including two major paleorivers. The depositional topography of these convergent fluvial fans would have inversely defined bathymetric lows during subsequent phases of lacustrine inundation, locations where trona could accumulate below a thermocline. Provenance mapping verifies fluvial connectivity to the Aspen paleoriver and to sources of alkalinity in the Colorado Mineral Belt across Wilkins Peak Member deposition, and shows that the greatest volumes of sediment were delivered from the Aspen paleoriver during deposition of marker beds A, B, D, and I, each of which were deposited coincident with prominent "hyperthermal" isotopic excursions documented in oceanic cores.

INTRODUCTION

Recent advances in the use of detrital geochronology to document sandstone provenance have revolutionized the analysis of ancient sedimentary depositional systems (Sharman et al., 2017; Leary et al., 2020; Parrish et al., 2023). Amassing detrital zircon and petrographic datasets large enough to characterize dynamic alluvial processes across entire basins, however, can be both time and cost prohibitive. Portable X-ray fluorescence (*p*XRF) devices offer a means to expand the reach of provenance studies to the landscape scale due to the low cost per analysis and rapid data acquisition in the field and laboratory. *p*XRF-generated elemental concentrations have been used as proxies for lithology, mineralogy, and provenance in ancient and modern sedimentary systems (Somarin, 2015; Chapman et al., 2021). Interpreting provenance from mineral proportions or elemental concentrations, however, can be challenging in ancient sedimentary deposits, due to differential weathering and abrasion of minerals, hydrodynamic sorting, authigenic mineral formation, and diagenesis (Odom et al., 1976; Garzanti et al., 2013). Well-preserved and documented terrestrial strata of the western United States provide a unique opportunity to place provenance data in a synoptic framework, which allows better recognition of sedimentary dynamics. Here, we exploit the thick, well-mapped, and precisely dated Green River Formation, Wyoming, USA, sedimentary archive using a high n, multivariate *p*XRF approach calibrated by traditional sandstone petrography.

The Wilkins Peak Member of the Green River Formation was deposited under endorheic lacustrine conditions between 51.6 Ma and 49.9 Ma (Smith et al., 2008a, 2010, 2015; Bruck et al., 2023), coincident with the ca. 53.3–49.1 Ma Early Eocene Climatic Optimum (EECO; Fig. 1; Zachos et al., 2001; Inglis et al., 2020). The EECO interval constitutes the most recent period of high, sustained temperatures and pCO_2 in geologic history (Zachos et al., 2008; Payros et al., 2015). Thus, properly interpreting its coeval depositional environments is crucial to uncovering this important analog for understanding landscape processes under greenhouse climatic conditions. We focus on developing an interpretive framework to document provenance changes in outcrops and core across the Green River Formation paleoclimatic archive.

This study seeks to evaluate and delineate detrital provenance in the Bridger sub-basin using a combination of sandstone petrography and *p*XRF analyses correlated to the Wilkins Peak Member. Across nine time slices spanning ~1.2 m.y., we document a dynamic interaction between river systems and the deposition of lacustrine evaporites in response to climatic change in the early Eocene greenhouse. More broadly, we demonstrate the efficacy of *p*XRF in helping to establish detailed provenance relations at temporal and spatial resolutions that would be prohibitively time-consuming or costly to achieve using either sandstone petrography or detrital geochronology alone.

Background

Paleogene lacustrine strata of the Green River Formation occur within the Greater Green River Basin, Piceance Creek Basin, and Uinta Basin

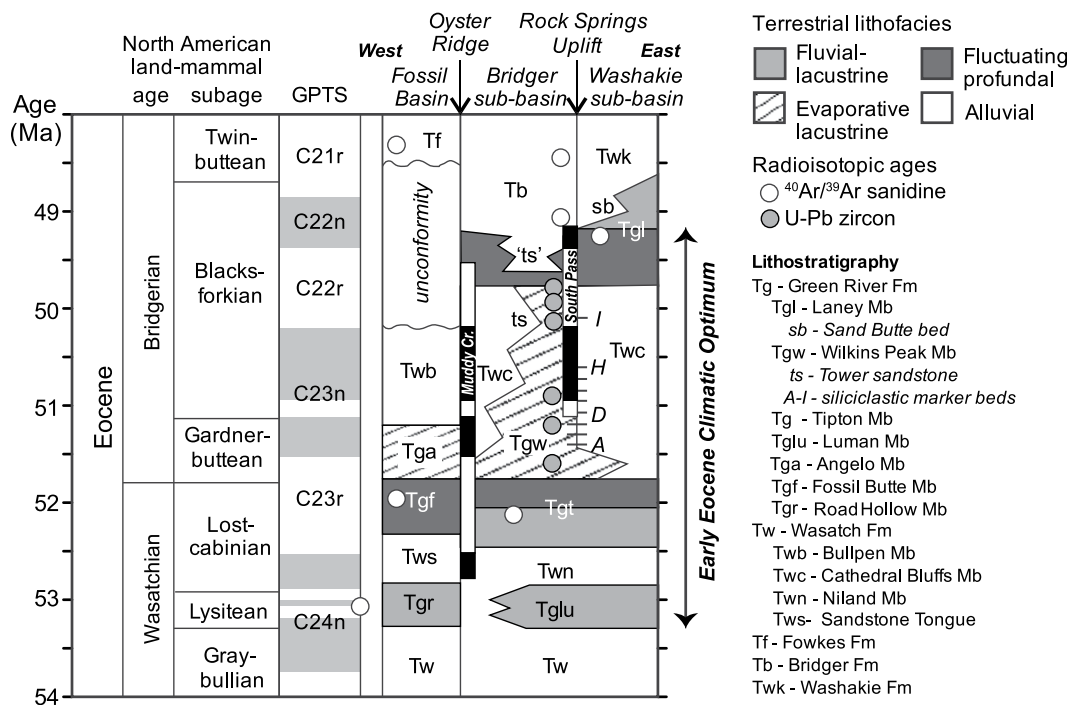M.E. Smith ⬤ https://orcid.org/0000-0001-6861-9342
†michael.e.smith@nau.edu

Figure 1. Time scale showing age context for Wilkins Peak Member, Wyoming, USA; U-Pb ages of tuff beds are from Bruck et al. (2023). $^{40}Ar/^{39}Ar$ ages of Smith et al. (2008a, 2010) are shown relative to the 28.201 Ma age for Fish Canyon sanidine (Kuiper et al., 2008). Paleomagnetic stratigraphy is from Muddy Creek (Zonneveld et al., 2003) and South Pass (Clyde et al., 2001). Duration of the Early Eocene Climatic Optimum follows Inglis et al. (2020). GPTS—geomagnetic polarity time scale; Fm—Formation; Mb—Member.

(Fig. 2), all of which formed due to Late Cretaceous through Paleogene contraction of the North American Cordillera and contemporaneous tectonic partitioning of its broad foreland by Laramide-style, basement-cored uplifts (Dickinson et al., 1988; DeCelles, 2004; Liu et al., 2005; Yonkee and Weil, 2015). The Wilkins Peak Member is composed of evaporative lake facies (Carroll and Bohacs, 1999) that accumulated in a closed lake system that precipitated voluminous evaporite minerals (Burnside and Culbertson, 1979; Smith et al., 2008b), including the world's largest soda ash (trona) deposits (Dyni, 1996) and significant volumes of halite. Sodium-carbonate evaporite deposits are rare in the geologic record, primarily because they evolve from uncommon parent waters in which $[HCO_3^- + CO_3^{2-}]$ initially exceeds $[Ca_2^+ + Mg_2^+]$ (Eugster and Hardie, 1978; Lowenstein et al., 2017).

The Wilkins Peak Member crops out along a 100-km-long, 20-km-wide escarpment on the eastern edge of the Bridger sub-basin of the Greater Green River Basin that exposes a unique cross section of a terminal distributive fan complex. Lithofacies in the middle and upper Wilkins Peak Member alternate between lacustrine and alluvial lithofacies at ~10–30 m vertical spacing in the Bridger sub-basin (Fig. 3C; Culbertson, 1961; Smoot, 1983; Smith et al., 2014a). Siliciclastic marker beds of the Wilkins Peak Member mark intervals of lowered lake level, when clastic advection carried sediment into the basin center, whereas the intervening lacustrine intervals record raised lake level and carbonate and evap-

orite deposition (Culbertson, 1961; Pietras and Carroll, 2006; Smith et al., 2014a). Radioisotopic geochronology of tuff beds interbedded within the Green River Formation and astrochronologic analysis of sedimentary cyclicity demonstrate that this alternation occurred, on average, every 100 k.y., which is consistent with short eccentricity cycles (Smith et al., 2010; Aswasereelert et al., 2013; Machlus et al., 2015; Bruck et al., 2023). Geochronology also indicates that several of the siliciclastic marker beds were deposited coeval with negative $\delta^{13}C$ and $\delta^{18}O$ excursions recorded in marine cores, which have been interpreted to record global "hyperthermal" events of atmospheric CO_2 (Lauretano et al., 2018; Bruck et al., 2023). Strata of the Wilkins Peak Member in the Bridger sub-basin are asymmetric, thickening southward toward the Uinta Uplift, which was active from the Late Cretaceous through the early Eocene (Bradley, 1964; Beck et al., 1988; Roehler, 1992; Fig. 3C). The Wilkins Peak Member was deposited contemporaneously with alluvial strata of the Wasatch Formation that surrounds lake deposits of the Wilkins Peak Member. Adjacent to the Uinta Uplift, Wilkins Peak Member strata interfinger with aerially restricted conglomeratic to quartzose, sand-rich alluvial fan deposits of the Cathedral Bluffs Member of the Wasatch Formation sourced from the Uinta Uplift (Powell, 1876; Crews and Ethridge, 1993; Smith et al., 2015; Fig. 3C). Coarse-grained facies of the Cathedral Bluffs Member of the Wasatch Formation also occur adjacent to the Wind River and Granite Mountains uplifts

(Pipiringos, 1955; Love, 1970; Roehler, 1993). Thick intervals of finer-grained and more voluminous alluvial channel- and floodplain-deposited strata from the Cathedral Bluffs Member of the Wasatch Formation are preserved in the Great Divide, Washakie, Sand Wash, and western Bridger sub-basin (Fig. 3D; Pipiringos, 1955; Sullivan, 1985; Roehler, 1992; Zonneveld et al., 2003; Smith et al., 2015). Upper Wilkins Peak Member-equivalent deltaic sandstone beds in the subsurface of the Bridger sub-basin were informally mapped as Tower sandstone (Fig. 1; Tofte and Carroll, 2022), which differ in age from homonymous Tower sandstone beds that occur within the lower Laney Member and crop out near Green River, Wyoming (Culbertson, 1962; Bradley, 1964). At the western edge of the Bridger sub-basin is Fossil Basin, a piggyback sub-basin of the Greater Green River Basin within the eastern Sevier fold-and-thrust belt (Fig. 2). Fossil basin evaporative lacustrine strata coeval to the Wilkins Peak Member are assigned to the lacustrine Angelo Member of the Green River Formation and are overlain by the alluvial Cathedral Bluffs Member-equivalent Bullpen Member of the Wasatch Formation (Oriel and Tracey, 1970; Buchheim et al., 2011; Fig. 1).

The Wilkins Peak Member accumulated within Eocene Gosiute Lake (King, 1878; Bradley, 1929) during a prolonged interval of regional hydrologic closure that began when a paleoriver that drained the Cordilleran hinterland in Idaho was diverted northward away from the Greater Green River Basin and into the Bighorn and
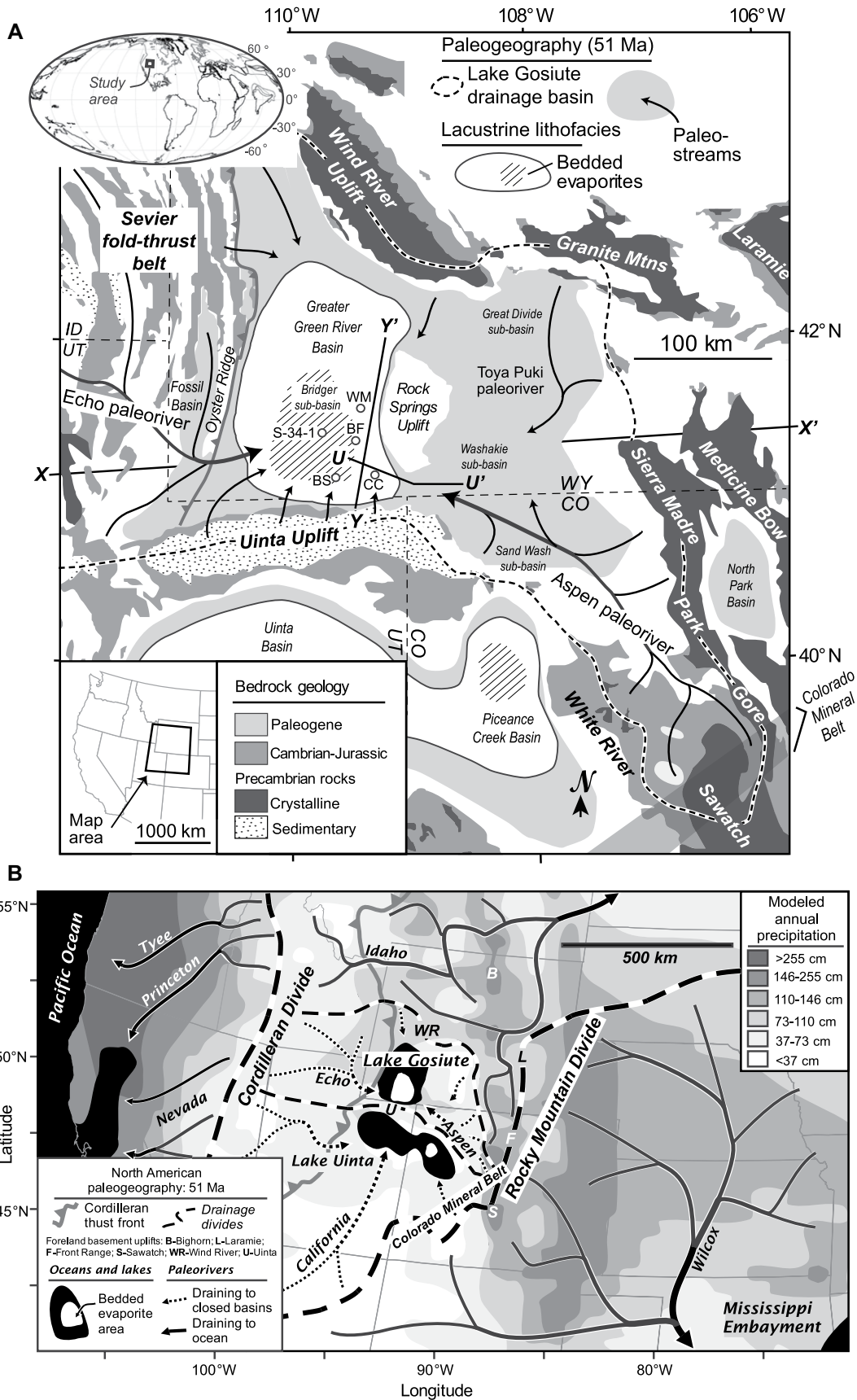
Figure 2. (A) Map of the Greater Green River Basin, Wyoming, USA, and surrounding region of the central Rocky Mountains, with the Wilkins Peak Member outlined in the Bridger sub-basin; includes inset global map showing study location relative to Eocene paleogeography. Modified from Smith et al. (2015). BF—Blacks Fork 1 core; BS—Baker-Smedley 1 core; CC—Currant Creek Ridge 1 core; WM—White Mountain 1 core. (B) Early Eocene paleogeography of the western United States, showing lakes (Smith et al., 2008), drainage divides (Henry et al., 2012; Smith et al., 2014b; Sharman et al., 2017), and modeled annual precipitation of Sewall and Sloan (2006). Modified from Smith et al. (2014a).
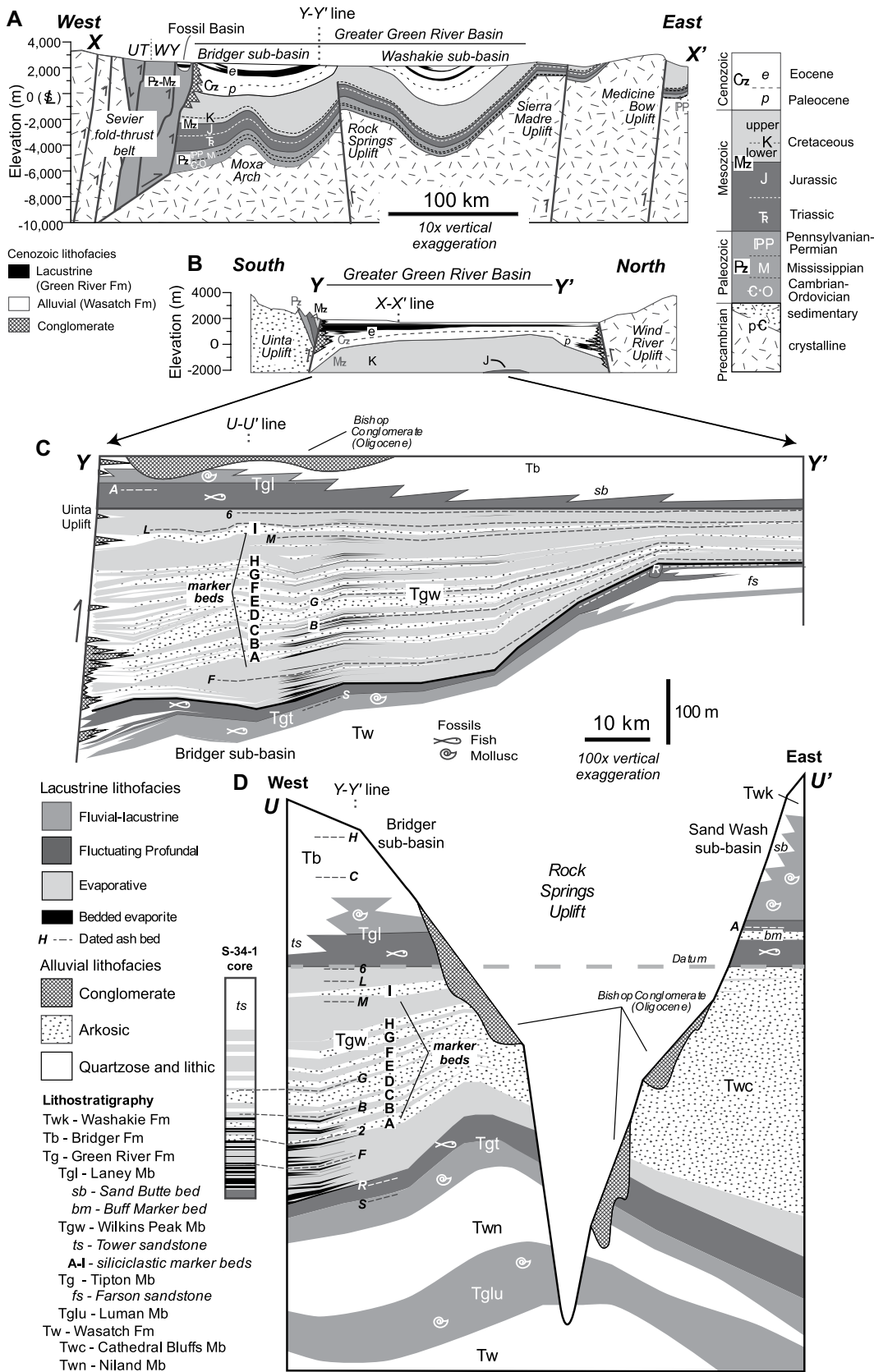
Figure 3. Cross sections of the study area modified from Smith et al. (2015). (A) W–E regional cross section; (B) S–N cross section; (C) detailed SE–NW; and (D) N–S cross sections of the Green River and Wasatch formations in the Greater Green River Basin, Wyoming, USA, showing stratigraphic context and extent of Wilkins Peak Member siliciclastic marker beds and radioisotopic geochronology. Strata were projected to a datum at the top of the Wilkins Peak Member. Radioisotopically dated ash beds: S—Scheggs; R—Rife; F—Firehole; 2—Second; B—Boar; G—Grey; M—Main; L—Layered; 6—Sixth; A—Analcite; C—Church Buttes; H—Henrys Fork (Smith et al., 2008a, 2010; Bruck et al., 2023).
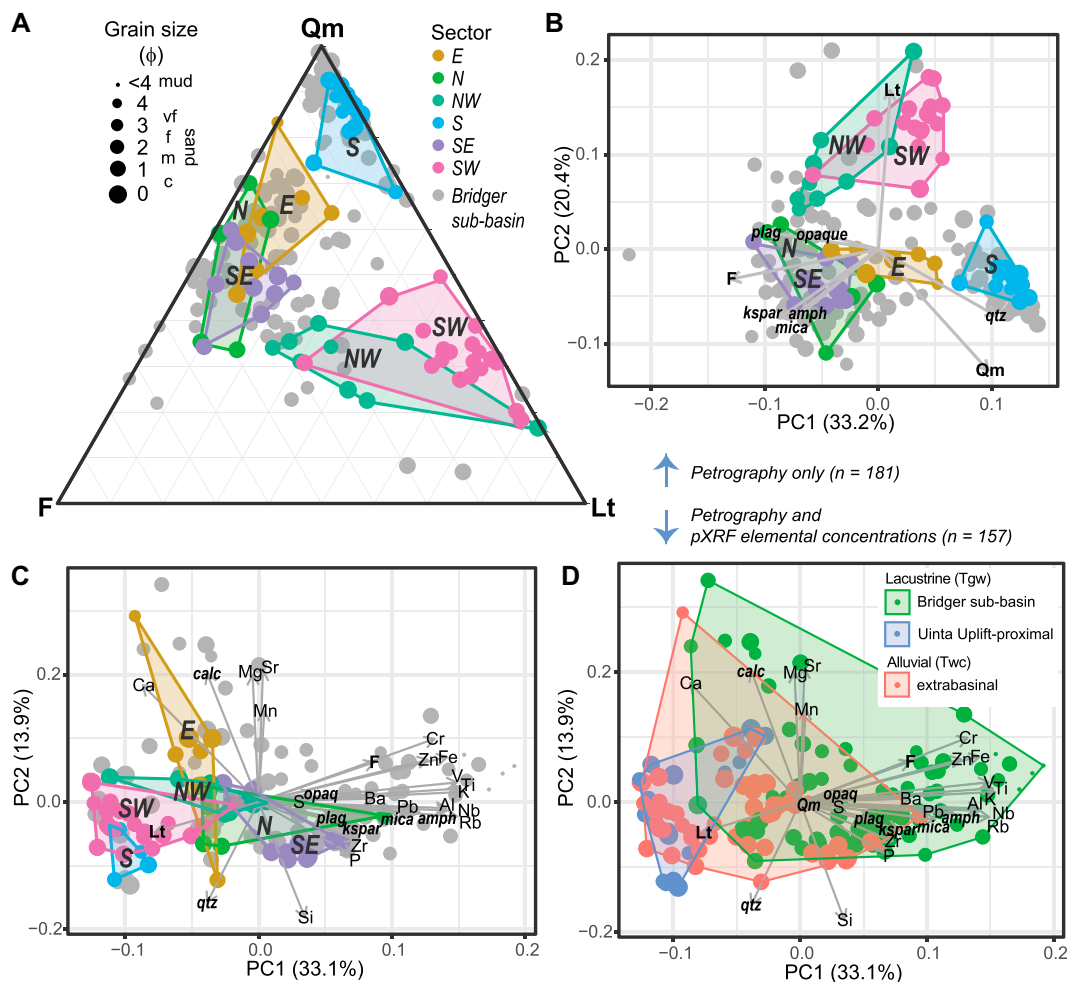
Figure 4. Thin section point-count results plotted on (A) monocrystalline quartz–feld-spar–total lithic (Qm-F-Lt) diagram following the Gazzi-Dickinson method (Dickinson, 1970; Zuffa, 1980; Ingersoll et al., 1984); (B) principal component analysis of sandstone mineral percentages for comparison; (C) principal component analysis of all X-ray fluorescence and petrography data pairs labeled by sector; and (D) lithofacies. Loadings for each individual element and grain type are shown with arrows. amph—amphibole; calc—calcite; F—feldspar; kspar—K-feldspar; plag—pla-gioclase; Qm—monocrystalline quartz.

Wind River basins (Pietras et al., 2003; Carroll et., 2008; Smith et al., 2014b; Honig, 2020). General circulation models of the North American Laramide foreland suggest that the Green River Formation lakes occupied a relatively dry, low-elevation intermontane region between the Rocky Mountains to the east and the crest of the North American Cordillera to the west (Fig. 2B; Sewall and Sloan, 2006; Walters et al., 2023). This region received runoff from precipitation that originated from both the Pacific Ocean and the Mississippian Embayment of the Gulf of Mexico (Fig. 4; Sewall and Sloan, 2006). Two relatively invariant drainage divides defined this closed region during the early Eocene: a Cordilleran divide that followed the crest of the retroarc hinterland in a N–S direction (Henry et al., 2012; Cassel et al., 2014), and a Rocky Mountain divide that followed Laramide basement structures northeastward from southwestern Colorado, USA, to western South Dakota, USA (Smith et al., 2014b; Sharman et al., 2017). During Wilkins Peak Member deposition, Gosiute Lake was situated between these divides and was hydrologically separated from the adjacent foreland region by

the east–west-trending ranges to the north and south (Figs. 2 and 4). Two extrabasinal streams, the Aspen and Echo paleorivers, flowed into Gosiute Lake from the southeast and west, respectively, and intermingled with clastic sediment emanating from local uplifts (Hammond et al., 2019; Parrish et al., 2023; Schwaderer, 2022). The Aspen paleoriver drained the western slopes of the Rocky Mountains and was a major source of arkosic siliciclastic detritus to the Sand Wash and Washakie sub-basins and eastern Bridger sub-basin. It drained northwestward into Gosiute Lake from the Rocky Mountain divide (Fig. 2B; Smith et al., 2008b, 2014b; Hammond et al., 2019; Parrish et al., 2023) and is hypothesized to have delivered requisite volcanogenic alkalinity to Gosiute Lake that supported the accumulation of trona in the Wilkins Peak Member (Lowenstein et al., 2017; Hammond et al., 2019; Arnuk et al., 2023). The Echo paleoriver emptied eastward into Gosiute Lake from the Cordillera and delivered sediment eroded from the Sevier thrust belt and the Cordilleran hinterland to the west (Oriel and Tracey, 1970; DeCelles, 1994; Baddouh et al., 2016; Schwaderer, 2022).

METHODS

Stratigraphy and Sampling

Eocene sedimentary lithofacies were analyzed and sampled from across the Greater Green River Basin. To establish a more detailed stratigraphic framework and better understand the influence of lithofacies on elemental concentrations, we measured and sampled eight outcrop sections of the D and I marker beds of the Wilkins Peak Member, documenting grain size, sorting, and sedimentary structures (Krueger, 2017; Gipson, 2019). A Radiation Solutions RS-230 BGO gamma-ray spectrometer was used to acquire elemental concentrations of U, Th, and K at half-meter spacing at all measured outcrop sections. Five subsurface drill cores of the study interval were also analyzed (Blacks Fork 1, Currant Creek Ridge 1, White Mountain 1, Baker-Smedley 1, and Solvay S-34-1). Beds I and D were selected for closer examination and correlation due to being the most easily correlated beds of the outcrop belt (Krueger, 2017; Gipson, 2019). We also sampled siliciclastic

TABLE 1. PRINCIPAL COMPONENT ANALYSES OF SEDIMENTARY ROCK SAMPLES OF THE WILKINS PEAK MEMBER OF THE GREEN RIVER FORMATION, WYOMING, USA, SHOWING PROPORTION OF VARIANCE EXPLAINED BY EACH PRINCIPAL COMPONENT

Analysis	n	PC1 (%)	PC2 (%)	PC3 (%)	PC4 (%)	PC1 + PC2 (%)	PC1 loadings >20%	PC2 loadings >20%	PC3 loadings >20%
(1) Petrography only (Figs. 4A and 4B)	183	33.1	20.4	13.4	10.8	53.5	(+) Qm, qtz (−) F, kspar, plag, amph, mica	(+) Lt (−) Qm, qtz, amph, mica	(+) Qtz (−) Calc
(2) Petrography plus *p*XRF elemental abundances (Figs. 4C and 4D)	157	33.1	13.9	8.7	7.7	47.0	(+) Mica, amph, Al, Cr, Fe, K, Nb, Pb, Rb, Ti, V, Zn	(+) Calc, Ca, Mg, Mn, Sr (−) Qtz, Si,	(+) Qm, qtz (−) Lt, plag
(3) *p*XRF elemental abundances (Fig. 5)	1438	42.9	12.9	7.3	6.1	55.8	(+) Ca (−) Al, Cr, Fe, K, Nb, Rb, Ti, V, Zn	(+) Ca, Cr, Mg, Mn, Sr, Zn (−) Si, Zr	(+) S (−) Ba, Mg, Mn, P, Si, Zr
(4) *p*XRF- and outcrop gamma spectrometer–derived elemental abundance (Fig. S3 [see text footnote 1])	327	28.3	10.2	8.7	7.2	28.5	(+) gK, Al, Cr, Fe, K, Nb, Pb, Rb, Ti, V, Zn (−) Ca	(+) Si, Zr (−) gU, Ca, Cr, Mg, Sr	(+) gU, gTh, Bi, P (−) Mg
(5) Provenance-focused PCA (Fig. 6)	439	65.2	23.1	9.8	1.9	88.3	(+) K, Rb, Pb, Si	(+) Si	(+) K, Rb (−) Pb

Note: *p*XRF—portable X-ray fluorescence; PCA—principal component analysis. Mineral percentages: Qm—monocrystalline quartz; qtz—quartz; F—feldspar; kspar—K-feldspar; plag—plagioclase; amph—amphibole; calc—calcite; g—prefix indicates element was measured using an outcrop gamma spectrometer.

mudstone and sandstone from Wilkins Peak Member marker beds using a rock hammer at closely spaced (5–10 km) locales across the eastern Bridger sub-basin outcrop belt (Gregorich, 2021). Hand samples were collected from as many of the marker beds as possible across the outcrop belt, with an aim toward regular geographic coverage of sampling. These data were integrated with an extensive stratigraphic database for the Wilkins Peak Formation (Smith et al., 2015, and references therein). Sandstone samples representative of potential source areas were also collected from Eocene alluvial strata surrounding the Wilkins Peak Formation. In total, 138 thin sections of sedimentary lithofacies from outcrops and core, predominantly fine- to medium-grained sandstone, were point-counted (300–400 grains each) and plotted on a monocrystalline quartz–feldspar–lithic clasts (Qm-F-Lt) diagram (Fig. 4A; Table S1 in the Supplemental Material[1]) following a modified Gazzi–Dickinson protocol (Dickinson, 1970; Zuffa, 1980; Ingersoll et al., 1984).

Geochemistry

Rock samples, outcrops, and cores were analyzed using a handheld Niton XL3 GOLDD XRF analyzer for elemental concentrations of Al, Ba, Ca, Cr, Fe, K, Mg, Mn, Nb, P, Pb, Rb, S, Si, Sr, Ti, V, Zn, and Zr using secondary X-ray spectra generated from tested samples. The device was operated in "mining Cu/Zn" mode using the main, high, low, and light filter

for 30 s each per 120 s analysis. For measured field sections and cores, a single analysis was performed in situ at each half-meter of the rock strata analyzed (n = 1105 analyses). Intervals of the Wilkins Peak Member in the Blacks Fork 1, Currant Creek Ridge 1, White Mountain 1, and Baker-Smedley 1 cores were measured at the U.S. Geological Survey Core Research Center. Field-collected hand samples and Solvay S-34-1 core samples were analyzed in the laboratory using a Niton 430-032 mobile test stand (n = 334 hand samples). Analyses were typically performed on indurated rock; in the rare case of a fissile sample, loose material was placed in plastic cups with thin film for analysis in the test stand. Analyses were performed on three different fresh surfaces per sample, and elemental concentrations were averaged, with an average total analysis time per sample of 360 s. For the provenance-focused analysis described below, when multiple analyses of a particular bed at a particular location were acquired, elemental compositions of individual beds were averaged for that locality. Table S1 contains the complete analytical and lithologic details for each sample. To calibrate *p*XRF-derived concentrations and identify instrumental drift, NIST 2709c PP standard material, which is composed of dry, homogenized soil from the San Joaquin Valley of California, USA, was measured regularly alongside sediment samples. No significant drift occurred during the period of data collection. XRF core-scanning of siliciclastic intervals of the Wilkins Peak Member was completed using a third-generation Avaatech XRF core-scanner at the University of Wisconsin–Madison, USA. See Walters et al. (2023) for complete core-scanning analytical details.

We used principal component analysis (PCA) to evaluate *p*XRF elemental data in concert with petrographic point count data, and to better understand the relationship between mineralogy, composition, and sedimentary lithofacies. The

analysis was implemented in R using the *prcomp* function of the *stats* package. PCA is a multi-variate statistical method to reduce the dimensionality of a dataset containing a large number of correlated variables without losing any of the original information. New uncorrelated variables (principal components) are calculated for the input sample set that capture covariance among multiple elements (Jolliffe and Cadima, 2016). We conducted five individual PCAs to investigate varying combinations of petrographic point count data, *p*XRF elemental concentrations, and gamma-ray spectrometer-acquired concentrations of K, Th, and U (Table 1, Fig. S1). The first PCA includes only petrographic results (Fig. 4B), and the second includes all samples with both petrographic point counts and *p*XRF elemental concentrations (Figs. 4C and 4D). A third PCA includes all *p*XRF measurements (Figs. 5 and S2), the fourth PCA includes all co-determined *p*XRF measurements and gamma-ray spectrometer assays (Fig. S3), and the fifth PCA includes only sandstone samples and is focused on differentiating clastic provenance by including only elements that are minimally influenced by lacustrine environments and weathering (Fig. 6). Scree plots showing the relative proportion of variance explained by principal components for each analysis are shown in Figure S4. PC1 values from the provenance-focused PCA were used to construct synoptic maps for eight time slices using samples from the individual sandstone marker beds (Fig. 7). Solvay S-34-1 core-scanning XRF concentrations of K, Rb, Pb, and Si within Wilkins Peak Member marker beds (cf. Walters et al., 2023) were converted from counts to elemental concentrations using linear regressions of *p*XRF elemental concentrations and core-scanner counts for 20 co-sampled intervals (Fig. S5). These data were projected into the provenance-focused PCA coordinates using the *predict* function of the *stats* package in R and provide a continuous qualitative record
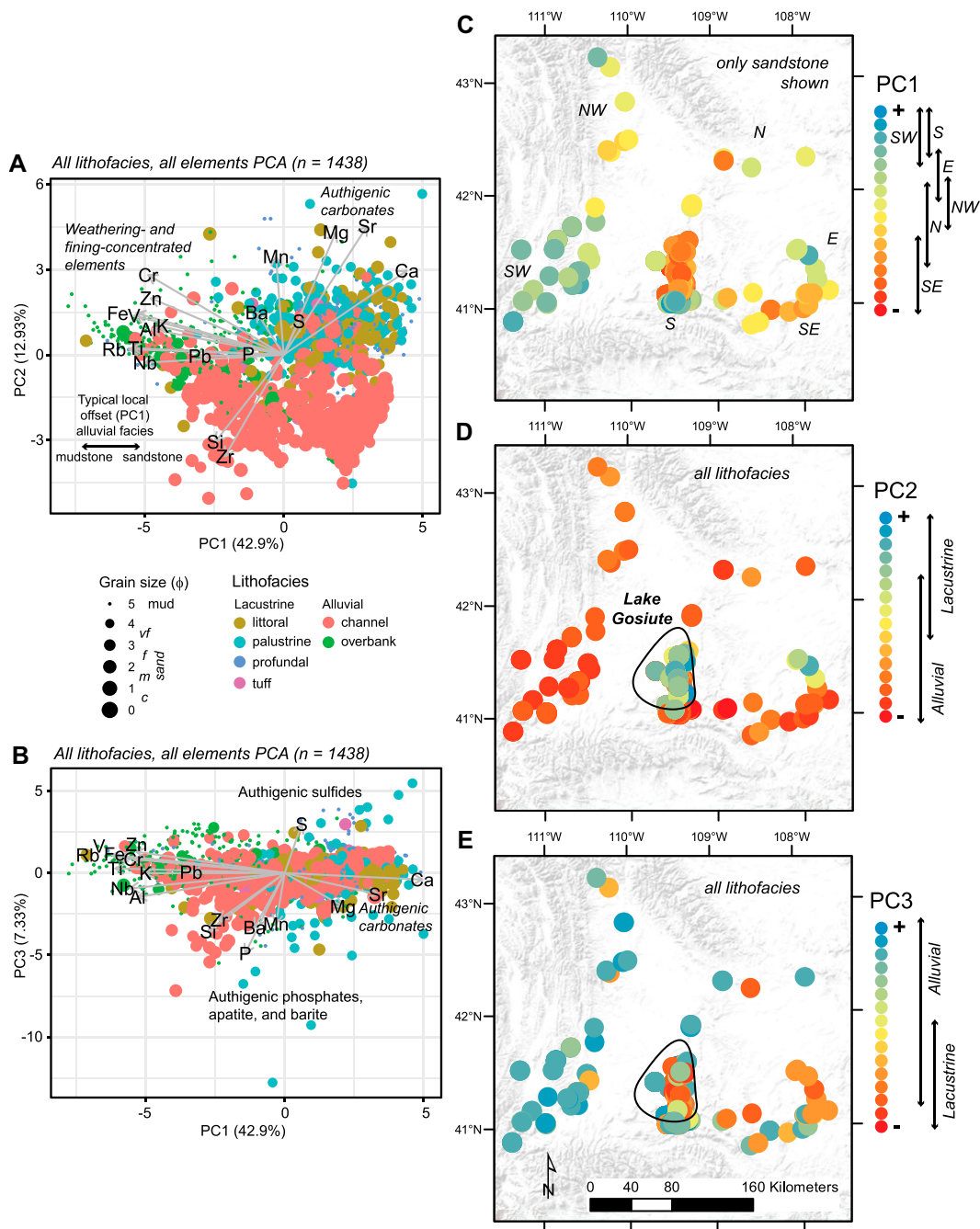
Figure 5. (A) Principal component analysis (PCA) of all portable X-ray fluorescence (*p*XRF)-measured samples showing PC1 and PC2 values and labeled according to lithofacies and grain size; (B) PCA of all *p*XRF-measured samples showing PC1 and PC3 values; (C–E) maps of PC1, PC2, and PC3 of values showing spatial relationships with catchment paleogeography and areal extent of Gosiute Lake.

of sediment provenance through the lower eight marker beds of the Wilkins Peak Member (beds A–H, Fig. 8C).

RESULTS

Sandstone Petrography

Point-count results of medium–fine-grained sandstone from across the Greater Green River Basin define three distinct compositional modes (Fig. 4A and Table S1). Sandstones are arkose to lithic arkose and often micaceous in the east-ern Bridger sub-basin and in sub-basins to the east of the Rock Spring Uplift, litharenite along the western edge of the Bridger sub-basin, and quartzose to litharenite adjacent to the Uinta Uplift. Within the modal size classes greater than very fine sand, sandstones are generally well sorted, with little evidence of mineralogy being dependent on grainsize (Fig. 5B). Lithic clasts in sandstones along the eastern edge of the Bridger subbasin are predominantly metamorphic, sedi-mentary, and volcanic in lithology, whereas clast lithologies are predominantly sedimentary along the western edge of the Bridger sub-basin and adjacent to the Uinta Uplift. Sandstones from the Bridger sub-basin often contain a higher percentage of lake-precipitated carbonate intra-clasts and cement, particularly adjacent to the Uinta Uplift (Smith et al., 2015). Sandstone modes in the basin are similarly differentiated in traditional ternary format (Fig. 4A) as they are by PCA values (Fig. 4B and Table 1).

Elemental Composition

Elemental concentrations assayed using *p*XRF for 1472 samples are influenced in several
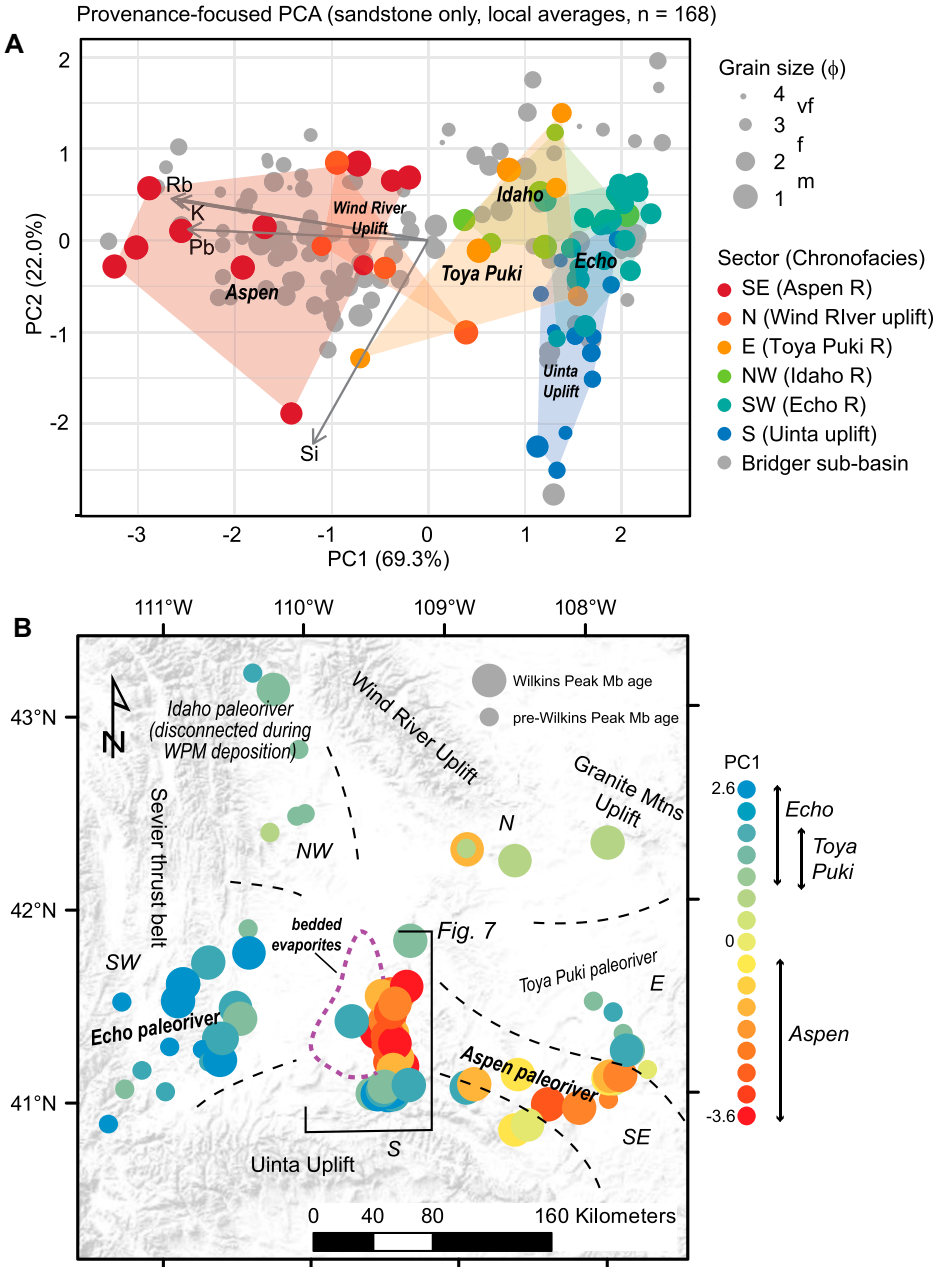
Figure 6. (A) Provenance-focused principal component analysis (PCA) results for sandstone samples, showing grouping by sector, and (B) mapped first principal component values for sandstone across the study area. Dashed lines show hypothesized boundaries of fluvial distributary fans originating in cardinal sectors surrounding Gosiute Lake.

ways by provenance, grain size, and sedimentary lithofacies. A correlation matrix created for 19 routinely detected elements shows strong correlations among several groups of elements with similar chemical characteristics (Fig. S1). We included all *p*XRF-detected elements and petrographic mineral percentages for 138 outcrop and core samples in a "petrography-*p*XRF" PCA (Figs. 4C and 4D; Table 1). The first principal component (PC1) explains 33.1% of the sample

variance and is highly influenced by a suite of elements common to feldspar, mica, amphibole, zircon, and rutile (K, Rb, Nb, Al, Pb, Ti, and Zr) and a suite of transition metals (Fe, V, Cr, and Zn), and is anticorrelated to the proportion of total lithic clasts (Lt) (Fig. 4C). The second principal component (PC2) accounts for 13.9% of the variance and is correlated to Sr, Ca, Mg, Mn, and calcite abundance, and anticorrelated to quartz and Si abundance (Fig. 4C), which is

consistent with higher carbonate content, meteoric carbonate cement, and lacustrine lithofacies (Fig. 4D).

A PCA that includes only XRF-measured elemental concentrations from 1470 samples (Fig. 5) illustrates similar lithofacies influences on elemental concentrations as those observed when only petrography was included (Fig. 4B). Within this analysis, PC1 accounts for 42.9% of the variance within the sample set, PC2 accounts for 12.9% of the variance, and PC3 accounts for 7.3% of the variance (Table 1). PC1 values for samples from the Bridger sub-basin are grouped into several distinct clusters that largely resemble the adjacent sectors of the paleocatchment. Most clastic sediment in the eastern Bridger sub-basin has negative PC1 values that resemble values for sandstone from the southeastern sector of the paleocatchment, which received sediment from the Aspen River (Fig. 5C). These sandstones contrast sharply with sandstone from the southwestern, southern, and eastern sectors of the paleocatchment, which have positive PC1 values.

Several elements (Ti, Al, Zr, Nb, Fe, Cr, Zn, V, and Cr) occur in greater concentration in samples from the Bridger sub-basin than in fluvial sandstone from all potential source areas (Fig. 5). These elements are most concentrated in fine-grained, silty-clay, siliciclastic mudstones within marker beds (Fig. 5A) that are interpreted, based on sedimentary structures and ichnofossils, to have been deposited in floodplain and littoral lacustrine settings (Smith et al., 2014a). Two-tailed t-tests of sandstone-mudstone pairs from 51 outcrops across the basin indicate a robust statistical dissimilarity between PC1 values (t = 5.542; p = 1.12e-06) and PC2 values (t = 4.187; p = 1.14e-04) for sandstone and mudstone samples from the same location and marker bed. These t-values well exceed the student's t critical values for dissimilarity. The mean differences in PC1 and PC2 between sandstone and co-sampled siliciclastic mudstone from specific locations were 2.10 and 1.36, respectively (Fig. 5A).

Lacustrine lithofacies diverge significantly from alluvial lithofacies along PC2, with positive loadings on Mg, Mn, Sr, and Ca, and negative loadings on Si and Zr (Fig. 5A), which is consistent with the presence of lake-precipitated authigenic minerals. Lacustrine lithofacies also diverge negatively in PC3 from a narrower population of fluvial channel and floodplain lithofacies based on greater concentrations of P, Ba, Si, Zr, and Mn, and positively based on elevated abundance of S (Fig. 5B). To further explore the mineralogy of Wilkins Peak Member lithofacies, a PCA was performed that includes both *p*XRF and gamma-ray spectrometer-measured ele-
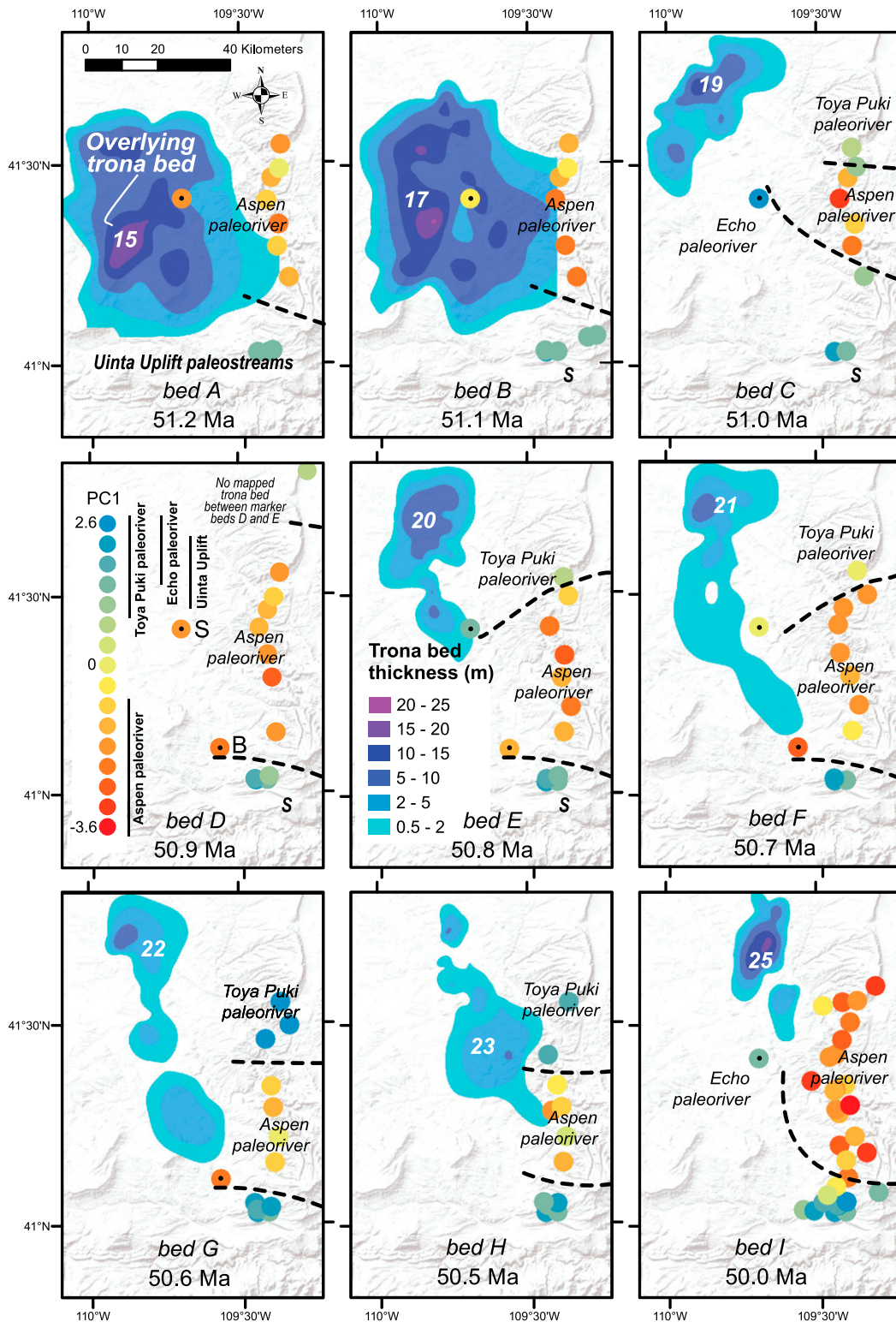
Figure 7. Repeat synoptic view of PC1 scores for siliciclastic marker beds A–I in SE Bridger sub-basin, showing the extent and thickness of evaporite beds in lacustrine beds immediately overlying each marker bed. Trona bed numbering follows Burnside and Culbertson (1979). Dashed lines indicate boundaries between different fluvial lobes and fans.

mental concentrations of K, U, and Th (Table 1 and Fig. S3). This PCA shows concordance of *p*XRF- and gamma-ray spectrometer-measured elemental concentrations of K. Gamma-ray spectrometer-measured U and Th elemental concentrations and *p*XRF-measured concentrations

of Bi and P load prominently on PC3 and are in greatest abundance in palustrine lithofacies.

The PCA shown in Figure 6A includes only XRF measurements of Si, K, Pb, and Rb from sandstone samples with modal grain sizes larger than very fine sand. These elements and grain

sizes are hypothesized to be least influenced by lacustrine, hydrodynamic, and pedogenic processes and products (see Discussion below for details concerning inclusion criteria for elements). Within this analysis, sandstone samples from six different geographic catchment sectors
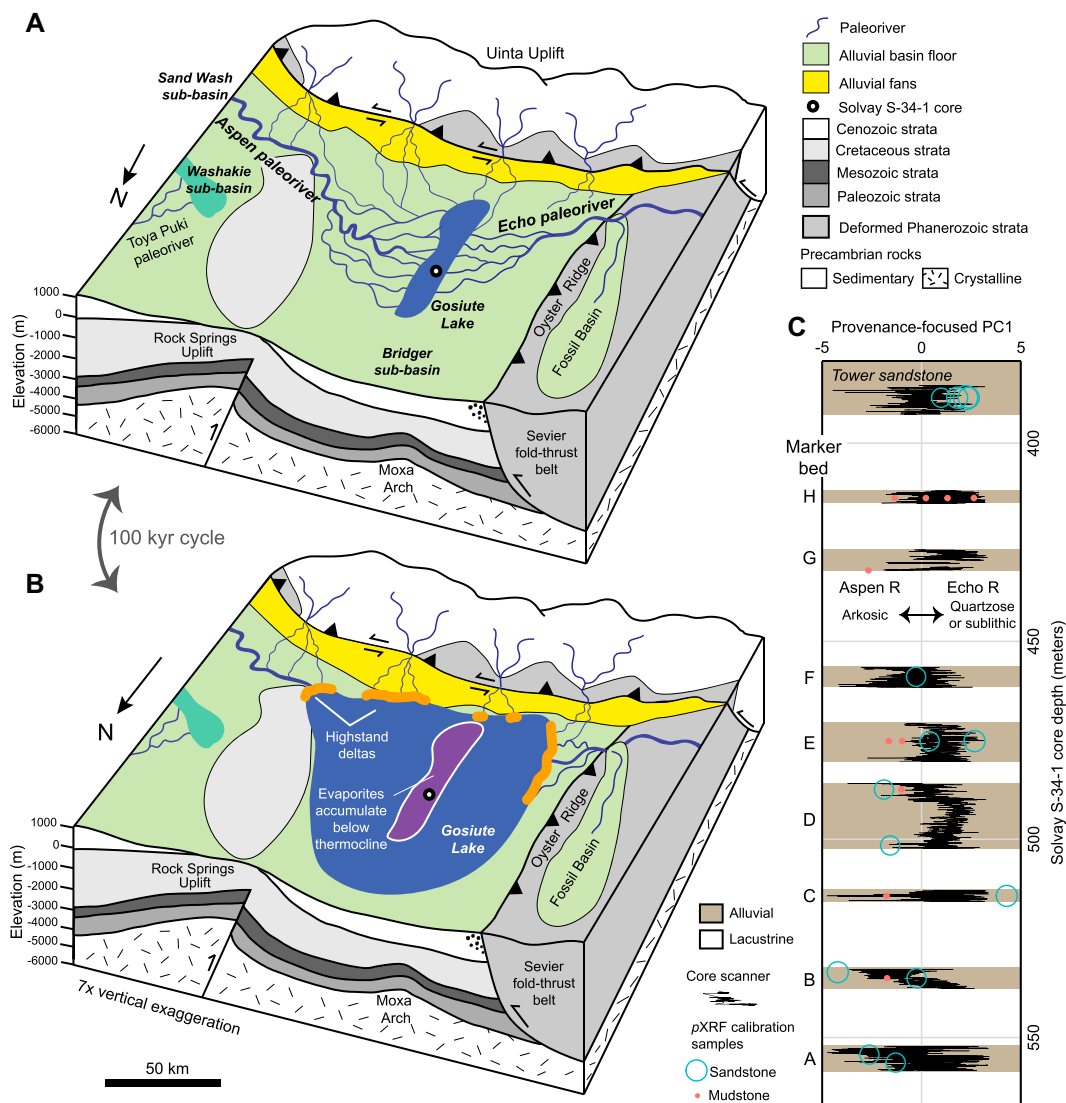
Figure 8. Perspective block diagrams showing (A) fluvial fans formed during lowstands of Gosiute Lake, Wyoming, USA, that deposited siliciclastic marker beds and (B) inundation by Gosiute Lake and evaporite beds formed in the resulting bathymetric deep during highstands. (C) Projected provenance-focused PC1 values for siliciclastic intervals of the Solvay S-34 core record from X-ray fluorescence (XRF) core scanning (see text), showing intra-bed variability and up-section shift from Aspen paleoriver to Echo paleoriver provenance across Wilkins Peak Member deposition. Blue and red marks indicate core samples that were analyzed with portable X-ray fluorescence (pXRF) and form the basis for the simple core scanner to pXRF value calibration that was used to project PC1 values for core scanner results (Fig. S5 [see text footnote 1]).

surrounding Gosiute Lake (SW, NW, N, E, SE, and S) plot as distinct clusters along PC1, and overlap with sandstone samples from the center of the Bridger sub-basin (Fig. 7A). These clusters broadly correspond to distinctive detrital zircon chronofacies (Parrish et al., 2023), which similarly depict the convergence of paleorivers and local drainages into Gosiute Lake. In the outcrop belt along the eastern edge of the Bridger sub-basin, a majority of samples have high K, Rb, and Pb concentrations and negative PC1 values that closely resemble those of sandstones from the SE sector (Fig. 6B), which implies derivation from the Aspen paleoriver. Sandstone samples from the southern and southwestern quadrants of the Gosiute Lake paleocatchment have lower K, Rb, and Pb concentrations and positive PC1 values that differ markedly from values for Aspen paleoriver-derived sandstone (Fig. 6B). Unfortunately, PC1

values do not differentiate Echo paleoriver and Uinta Uplift-derived clastic sediment. This similarity is present regardless of whether the elements excluded from the provenance-focused PCA are included or not (cf. Fig. 5C) and likely reflects the similar Proterozoic and Paleozoic bedrock that underlies the Sevier fold-thrust belt and the Uinta Uplift (Fig. 3). Nevertheless, Echo paleoriver and Uinta Uplift-derived clastic sediment are distinct in PC2 values (Fig. 6A), which is consistent with petrographic evidence for a higher proportion of lithic clasts in Echo paleoriver-derived sandstone (Fig. 4). Several sandstone samples from the northeast Bridger sub-basin have high PC1 values that resemble those of sandstones from the eastern sector of the paleocatchment (Fig. 6B), and are interpreted to have been fed by a Toya Puki paleoriver based on detrital zircon geochronology (Parrish et al., 2023).

In a temporal sequence of synoptic maps of each of the Wilkins Peak Member marker beds (Fig. 7), PC1 values illustrate the low PC1 distributary fan from the Aspen River competing with high PC1 distributary fans of the Echo and Toya Puki paleorivers and streams that drained the Uinta Uplift. Sandstone with compositions intermediate to the Aspen and other paleorivers generally only occurs on the edges of the fans within particular marker beds, which implies little interfan mixing. However, the apparent fan edges shifted laterally between successive marker beds. The A, B, D, and I marker beds record the broadest expansions of the Aspen River-sourced distributary fan across the outcrop belt. Marker beds C, G, and H, in contrast, mark the retrogradation and narrowing of the Aspen distributary fan. At the Solvay core location, to the west of the outcrop belt, Aspen River-derived sandstone is replaced up-section by sandstone

that is similar in composition to Echo River-derived sandstone (Fig. 8C), which is consistent with documented eastward progradation of its distributary fan (Fig. 3D). Projected PC1 values calculated from XRF-scanned elemental concentrations of K, Rb, Pb, and Si show prominent variations between and within individual marker beds within the S-34-1 core (Fig. 8C). In particular, beds A, B, and D record prominent intrabed shifts in PC1 from Echo River to Aspen River values upsection (Fig. 8C), which suggests a dynamic change in provenance during the deposition of particular marker beds. In the upper part of the S-34-1 core, deltaic sandstone lithofacies informally assigned to the Tower sandstone overlie lacustrine Wilkins Peak Member strata above the H marker bed (Figs. 3D, 7, and 8C). *p*XRF results show that this sandstone is compositionally distinct from both Aspen River-derived sandstone and the "Tower sandstone" beds that occur within the lower Laney Member of the Green River Formation near the town of Green River, Wyoming (Culbertson, 1962; Bradley, 1964).

DISCUSSION

The geological complexity of ancient strata makes provenance interpretation of sandstone composition more challenging than for modern settings (Smith et al., 2018; Chapman et al., 2021). In the case of the Green River Formation and related deposits, several interrelated mechanisms appear to have affected mineral and elemental abundances in a manner that obfuscates provenance interpretation, including: (1) grain size-dependent differences in mineral abundance, (2) authigenic minerals precipitated from lake or meteoric waters, and (3) differential chemical weathering, attrition, and/or sorting of minerals en route to the basin center. These mechanisms are expressed geochemically in samples from the basin center by a clear divergence from the range of elemental abundances observed in sandstone samples from source regions (Fig. 5). The resulting lack of "intermediacy" of elemental abundances within samples from the basin center makes certain nonconservative elements inappropriate candidates for provenance tracing. This makes typical nonparametric statistical tests used for element inclusion decision-making (i.e., the Mann-Whitney U test or Kruskal-Wallis H test; cf. Chapman et al., 2021) largely ineffective for ancient strata. The following account describes the reasoning for exclusion of grain sizes smaller than fine sand, and inclusion of only K, Rb, Pb, and Si elemental abundances in the provenance-focused PCA upon which

provenance interpretations and mapping of the Wilkins Peak Member in this study are based.

Grain Size

Finer-grained fractions from the same sediment source typically contain more feldspar than coarser-grained fractions, presumably due to cleavage and lower hardness (Odom et al., 1976) and a greater abundance of clay minerals. No clear bias in PC1 was observed in samples composed of fine–medium-grained to coarse-grained sandstone; however, samples finer than very fine sand exhibit a systematic −2.1 shift in PC1 value, on average, relative to sandstone sampled from the same outcrop (Fig. 5A). The effect is predominantly observed among samples with grain sizes smaller than very fine sand. The effect is diminished to an average difference of 0.73 for PC1 when only the limited suite of elements included in the provenance-focused PCA (K, Rb, Pb, and Si) is considered, but sandstone and mudstone samples remain distinguishable in a paired t-test (t = 3.54, df = 50, p = 0.00088) even within this framework. To avoid bias and inaccuracy, we excluded samples with grain sizes smaller than fine sand from the provenance-focused PCA (Fig. 6A), which was used to construct synoptic provenance-maps of individual marker beds (Fig. 7).

Authigenic Minerals

The Wilkins Peak Member contains a wide variety of sedimentary lithologies, including carbonate (calcite and dolomite) and evaporite minerals (trona, halite, and many others; Fahey, 1962; Smoot, 1983; Jagniecki and Lowenstein, 2015). Ca, Mg, Sr, and Mn contained in carbonate minerals likely cause the observed PC2 skew observed in lacustrine samples outside the range of possible clastic source compositions (Fig. 5A). Similarly, elevated U, Th, P, Ba, Mn, and Bi concentrations in some lacustrine samples inform a skew to negative PC3 values outside the range of potential source values (Figs. 5B and S2) and likely result, in part, in the presence of lacustrine phosphate minerals (Fahey, 1962; Mott and Drever, 1983). Anomalously high PC3 values associated with elevated S-elemental abundance occur in a subset of lacustrine lithofacies (Fig. 5B) and could signal the presence of lacustrine and/or diagenetic sulfide minerals. These minerals are abundant in organic-rich intervals of the Wilkins Peak Member due to salinity stratification-induced dysoxic bottom waters (Walters et al., 2023). To minimize the influence of authigenic minerals on provenance mapping, we excluded Ca, Mg, Sr, Mn, S, P, Ba, and Bi from the provenance-focused PCA.

Weathering and Winnowing

Significant systematic changes in mineral and elemental abundance can result from the weathering of minerals in sedimentary settings (Garzanti et al., 2013), particularly in warm environments, and can result in economically valuable "supergene" concentrations of metals, including Al, Fe, V, Ti, Zn, and Cr (Valeton, 1994). Sediment grains that were transported into Gosiute Lake from its paleocatchment likely underwent significant chemical weathering, particularly while temporarily stored in floodplain soil environments (Romans et al., 2016). This weathering would have been enhanced by high temperatures and atmospheric CO_2 concentrations that occurred during the Early Eocene Climatic Optimum (Smith et al., 2008b; Hyland and Sheldon, 2013). A related suite of minerals and elements can also be concentrated by hydraulic sorting in channels during fluvial transport, which can form placer-type clastic deposits rich in dense, durable, and/or weathering-resistant accessory minerals (i.e., zircon, muscovite, and rutile; cf. Garzanti et al., 2013). Sorting could, for example, account for elevated Zr, Nb, and Ti elemental abundance in some basin-center samples relative to possible source regions. To most effectively reduce the skew of PC1 values for basin-center samples outside the range of possible source compositions due to weathering and winnowing, we have excluded Fe, Al, V, Ti, Zn, Zr, Nb, and Cr from the provenance-focused PCA (Fig. 6). Note that while elimination of these elements from the provenance-focused PCA results in better overlap between source and basin-center sandstone (Fig. 6A), the inclusion of these elements (cf. Fig. 5C) produces very similar relative provenance distinctions.

Paleogeography, Paleogeomorphology, and Paleolimnology

Ancient Gosiute Lake received sediment from the distributary fans of two extrabasinal rivers systems and several smaller catchments that drained local uplifts during Wilkins Peak Member deposition (Fig. 6). These fluvial fans and distributary networks were profoundly affected by high-amplitude cyclic changes in lake level. Lithofacies stacking patterns show that the basin shifted between predominantly lacustrine conditions and alluvial conditions at the time scale of short eccentricity (Culbertson, 1961; Aswasereelert et al., 2013; Smith et al., 2014a; Bruck et al., 2023). During lacustrine intervals, the locus of deposition for the Aspen River sediments shifted updip due to rising lake level to the east of the Rock Springs Uplift (Fig. 8A), into the Washakie sub-basin (Smith et al., 2014a;

Hammond et al., 2019). During alluvial intervals, lake level dropped, and siliciclastic sediment was transported into the Bridger sub-basin (Fig. 8B), reestablishing a broad, low-relief distributary fan atop recently deposited carbonate lake sediment. Marker beds were deposited between 51.2 Ma and 50 Ma, respectively, and are hypothesized to correlate to global hyperthermal events (Bruck et al., 2023).

The edges of different distributary fans of the Aspen, Toya Puki, and Echo paleorivers, and fluvial fans originating in the Uinta Uplift shifted laterally between successive marker beds (Fig. 7). In the S-34-1 XRF-scanned core record and surface sections, provenance shifted from one lobe to another across the deposition of individual marker beds (Fig. 8C). The migrating northern and southern edges of the Aspen paleoriver distributary network are clearly defined across successive beds, which suggests minimal downstream mixing of sediment with other fluvial fans originating in the Uinta Uplift or the Toya Puki paleoriver(s) that drained the uplands formed by the Rawlins and Granite Mountains basement uplifts (Parrish et al., 2023). This contrasts with analog experiments that show more mixing between axial and transverse sediment sources due to erosion at the toe of steep transverse fan material by the axial stream (Connell et al., 2012). This discrepancy is likely due to fundamental differences in scale between analog experiments and paleolandscapes. We hypothesize that subtle but broad positive topographic relief due to sediment aggradation on fluvial distributary fans makes them less likely to mix at their edges. Accommodation of sediment in local basins likely also contributed to the lack of mixing between sediment streams. The Sand Wash sub-basin accumulated predominantly Aspen paleoriver-derived sediment (Fig. 2A), whereas the Washakie sub-basin trapped sediment from both the Toya Puki (Parrish et al., 2023) and Aspen paleorivers (Hammond et al., 2019). These basins likely acted as local sediment sinks that could have hindered sediment mixing en route to Gosiute Lake (Fig. 3D).

Marker beds A, B, D, and I record the greatest expansions of the distributary fan of the Aspen paleoriver (Fig. 7). These beds thus record the highest rates of sediment advection from the Aspen River paleocatchment, which drained the western slopes of the Rocky Mountains in northern Colorado (Fig. 2B). High-precision U-Pb geochronology for Wilkins Peak Member tuff beds shows that these beds correspond to three of the most prominent isotopic excursions in the marine record (Lauretano et al., 2018; Bruck et al., 2023). Their correspondence is consistent with hyperthermal events preferentially enhancing sediment advection from the Rocky Moun-

tains and Aspen River relative to other parts of Gosiute Lake's paleocatchment.

Sandstone from the Echo River is poorly represented in the outcrop belt and cores in the eastern Bridger sub-basin, but presumably underlies much of the western Bridger sub-basin (Sullivan, 1985; Zonneveld et al., 2003; Tofte and Carroll, 2022). The Echo distributary fan appears to have prevailed over the Aspen River fan at the Solvay core location in the central Bridger sub-basin by middle-Wilkins Peak Member time (Fig. 8C). Eastward progradation of the Echo paleoriver distributary fan was promoted by fluvial bypass when Fossil Basin was integrated into the Sevier wedge top by east-vergent uplift along the Hogsback thrust (Yonkee and Weil, 2015). This integration occurred roughly coincident with deposition of the fluvial Bullpen Member of the Wasatch Formation in Fossil Basin (Oriel and Tracey, 1970; Buchheim et al., 2011), Cathedral Bluffs Member fluvial strata in the western Bridger sub-basin (Sullivan, 1985; Zonneveld et al., 2003), and the lacustrine middle and upper Wilkins Peak Member in the central and eastern Bridger sub-basin (Fig. 1). Following spillover, Echo River detritus could flow directly into the western and central parts of the Bridger sub-basin to construct a fluvial distributary fan (Oriel and Tracey, 1970; Zonneveld et al., 2003; Buchheim et al., 2011; Tofte and Carroll, 2022). The eastern edge of the Echo distributary fan delivered sand to the western shores of Gosiute Lake that is assigned to the Tower sandstone in the subsurface of the central Bridger sub-basin (Fig. 7).

Comparison of *p*XRF-based provenance mapping of Wilkins Peak Member marker beds and evaporite occurrence in directly overlying lacustrine intervals shows that fluvial distributary fan topography and evaporite occurrence often appear to be an inverse image of one another (Fig. 7). This could suggest that fan topography framed a deep pool that could stay below the thermocline and where evaporite minerals could be preserved (Fig. 8B). Solutes would have been delivered up-dip to Gosiute Lake by rivers during lacustrine highstands, but evaporite minerals were not preserved across the entire area of inundation by Gosiute Lake and are instead preserved in relatively discrete areas in the center of the Bridger sub-basin (Fig. 7). Such evaporite focusing is hypothesized to occur because during summers, preservation of lacustrine evaporites is highly sensitive to dissolution above a thermocline (Demicco and Lowenstein, 2020). The pattern of shifting evaporite beds in this scenario would largely be defined by the balance of tectonic accommodation, and the volume and geometry of sediment delivery by competing fluvial systems.

CONCLUSIONS

Basin-scale, large sample-size *p*XRF analysis was performed on well-dated cyclic strata of the Green River Formation, and yields results comparable to sandstone petrography and detrital zircon geochronology but with a much higher sampling density. Principal component analysis (PCA) and comparison to lithofacies characteristics allows the isolation of several elements most useful for provenance analysis (K, Rb, Pb, and Si) from a broader suite of elements that are more heavily influenced by authigenic minerals, grain-size reduction, chemical weathering, and winnowing. PCA-based mapping of compositional modes defines the waxing and waning of two competing distributary fans from the Aspen and Echo paleorivers and several smaller fans fed by streams originating from local uplifts. Sharp lateral boundaries between provenance-defined fan lobes suggest minimal mixing between fluvial fans. At some locations, sediment sources appear to have changed abruptly during the deposition of individual beds. Marker beds A, B, D, and I represent the greatest expansions of the Aspen River distributary fan surface and appear to have been deposited during prominent global isotopic events recorded in oceanic cores. The Aspen distributary fan was displaced eastward by the Elko distributary fan across Wilkins Peak Member deposition. This resulted in a major up-section change in sand composition to Echo paleoriver values in the basin-center Solvay S-34-1 paleoclimatic archive. Evaporite beds between marker beds often occur in inverse spatial relation with Aspen and Echo distributary fan topography, which may imply that their composite topography acted to bathymetrically frame a deep pool that could stay below the thermocline to accumulate and preserve evaporite minerals.

REFERENCES CITED

Arnuk, W.D., Lowenstein, T.K., Klonowski, E.M., Carroll, A.R., and Smith, M.E., 2023, Simulating the source waters for the Wilkins Peak Member evaporite sequence with modern soda spring analogues: Applied Geochem-

istry, v. 151, https://doi.org/10.1016/j.apgeochem.2023.105597.

Aswasereelert, W., Meyers, S.R., Carroll, A.R., Peters, S.E., Smith, M.E., and Feigl, K.L., 2013, Basin-scale cyclostratigraphy of the Green River Formation, Wyoming: Geological Society of America Bulletin, v. 125, p. 216–228, https://doi.org/10.1130/B30541.1.

Baddouh, M., Meyers, S.R., Carroll, A.R., Beard, B.L., and Johnson, C.M., 2016, Lacustrine 87Sr/86Sr as a tracer to reconstruct Milankovitch forcing of the Eocene hydrologic cycle: Earth and Planetary Science Letters, v. 448, p. 62–68, https://doi.org/10.1016/j.epsl.2016.05.007.

Beck, R.A., Vondra, C.F., Filkins, J.E., and Olander, J.D., 1988, Syntectonic sedimentation and Laramide basement thrusting, Cordilleran foreland; Timing of deformation, in Schmidt, C.J., and Perry, W.J., Jr., eds., Interaction of the Rocky Mountain Foreland and the Cordilleran Thrust Belt: Geological Society of America Memoir 171, p. 465–488, https://doi.org/10.1130/MEM171-p465.

Bradley, W.H., 1929, The varves and climate of the Green River epoch: U.S. Geological Survey Professional Paper 158-E, p. 87–110.

Bradley, W.H., 1964, The geology of the Green River Formation and associated Eocene rocks in southwestern Wyoming and adjacent parts of Colorado and Utah: U.S. Geological Survey Professional Paper 496-A, p. 1–86, https://doi.org/10.3133/pp496A.

Bruck, B.T., Singer, B.S., Schmitz, M.D., Carroll, A.R., Meyers, S., and Walters, A., 2023, Astronomical and tectonic influences on climate and deposition of the Early Eocene Green River Formation, Wyoming: Geological Society of America Bulletin, v. 135, p. 3173–3182, https://doi.org/10.1130/B36584.1.

Buchheim, H.P., Cushman, R.A., and Biaggi, R.E., 2011, Stratigraphic revision of the Green River Formation in Fossil Basin, Wyoming: Overfilled to underfilled lake evolution: Rocky Mountain Geology, v. 46, p. 165–181, https://doi.org/10.2113/gsrocky.46.2.165.

Burnside, M.J., and Culbertson, W.C., 1979, Trona deposits in the Green River Formation, Sweetwater, Uinta, and Lincoln Counties, Wyoming: U.S. Geological Survey Open-File Report 79-737, p. 1–10.

Carroll, A.R., and Bohacs, K.M., 1999, Stratigraphic classification of ancient lakes: Balancing tectonic and climatic controls: Geology, v. 27, p. 99–102, https://doi.org/10.1130/0091-7613(1999)027<0099:SCOALB>2.3.CO;2.

Cassel, E.J., Breecker, D.O., Henry, C.D., Larson, T.E., and Stockli, D.E., 2014, Profile of a paleo-orogen: High topography across the present-day Basin and Range from 40 to 23 Ma: Geology, v. 42, p. 1007–1010, https://doi.org/10.1130/G35924.1.

Chapman, K.A., et al., 2021, Estimating the contribution of tributary sand inputs to controlled flood deposits for sandbar restoration using elemental tracers, Colorado River, Grand Canyon National Park, Arizona: Geological Society of America Bulletin, v. 133, p. 1141–1156, https://doi.org/10.1130/B35642.1.

Clyde, W.C., Sheldon, N.D., Koch, P.L., Gunnell, G.F., and Bartels, W.S., 2001, Linking the Wasatchian/Bridgerian boundary to the Cenozoic global climate optimum: New magnetostratigraphic and isotopic results from South Pass, Wyoming: Palaeogeography, Palaeoclimatology, Palaeoecology, v. 167, p. 175–199, https://doi.org/10.1016/S0031-0182(00)00238-8.

Connell, S.D., Kim, W., Smith, G.A., and Paola, C., 2012, Stratigraphic architecture of an experimental basin with interacting drainages: Journal of Sedimentary Research, v. 82, p. 326–344, https://doi.org/10.2110/jsr.2012.28.

Crews, S., and Ethridge, F., 1993, Laramide tectonics and humid alluvial fan sedimentation, NE Uinta Uplift, Utah and Wyoming: Journal of Sedimentary Research, v. 63, p. 420–436, https://doi.org/10.1306/D4267B18-2B26-11D7-8648000102C1865D.

Culbertson, W.C., 1961, Stratigraphy of the Wilkins Peak Member of the Green River Formation, Firehole Basin quadrangle, Wyoming: U.S. Geological Survey Professional Paper 424-D, p. 170–173.

Culbertson, W.C., 1962, Laney Shale Member and Tower Sandstone Lentil of the Green River Formation, Green River area, Wyoming: U.S. Geological Survey Professional Paper 449-C, p. 54–57.

DeCelles, P.G., 1994, Late Cretaceous-Paleocene synorogenic sedimentation and kinematic history of the Sevier thrust belt, northeast Utah and southwest Wyoming: Geological Society of America Bulletin, v. 106, p. 32–56, https://doi.org/10.1130/0016-7606(1994)106<0032:LCPSSA>2.3.CO;2.

DeCelles, P.G., 2004, Late Jurassic to Eocene evolution of the Cordilleran thrust belt and foreland basin system, western U.S.A.: American Journal of Science, v. 304, p. 105–168, https://doi.org/10.2475/ajs.304.2.105.

Demicco, R.V., and Lowenstein, T.K., 2020, When "evaporites" are not formed by evaporation: The role of temperature and pCO2 on saline deposits of the Eocene Green River Formation, Colorado, USA: Geological Society of America Bulletin, v. 132, p. 1365–1380, https://doi.org/10.1130/B35303.1.

Dickinson, W.R., 1970, Interpreting detrital modes of greywacke and arkose: Journal of Sedimentary Petrology, v. 40, p. 695–707.

Dickinson, W.R., Klute, M.A., Hayes, M.J., Janecke, S.U., Lundin, E.R., McKittrick, M.A., and Olivares, M.D., 1988, Paleogeographic and paleotectonic setting of Laramide sedimentary basins in the central Rocky Mountain region: Geological Society of America Bulletin, v. 100, p. 1023–1039, https://doi.org/10.1130/0016-7606(1988)100<1023:PAPSOL>2.3.CO;2.

Dyni, J.R., 1996, Sodium carbonate resources of the Green River Formation: U.S. Geological Survey Open-File Report 96–729, 39 p.

Eugster, H.P., and Hardie, L.A., 1978, Saline lakes, in Lerman, A., ed., Lakes: Chemistry and Geology: New York, Springer, p. 237–293, https://doi.org/10.1007/978-1-4757-1152-3_8.

Fahey, J.J., 1962, Saline minerals of the Green River Formation: U.S. Geological Survey Professional Paper 405, p. 1–50.

Garzanti, E., Padoan, M., Andò, S., Resentini, A., Vezzoli, G., and Lustrino, M., 2013, Weathering and relative durability of detrital minerals in equatorial climate: Sand petrology and geochemistry in the East African Rift: The Journal of Geology, v. 121, p. 547–580, https://doi.org/10.1086/673259.

Gipson, L.A., 2019, Early Eocene paleogeomorphology of an alluvial system within the Wilkins Peak Member of the Green River Formation, Wyoming [M.Sc. thesis]: Flagstaff, Arizona, Northern Arizona University, 98 p.

Gregorich, H.G., 2021, Provenance analysis of siliciclastic beds of the Wilkins Peak Member of the lower Eocene Green River Formation, Wyoming [M.Sc. thesis]: Flagstaff, Arizona, Northern Arizona University, 100 p.

Hammond, A.P., Carroll, A.R., Parrish, E.C., Smith, M.E., and Lowenstein, T.K., 2019, The Aspen paleoriver: Linking Eocene magmatism to the world's largest Na-carbonate evaporite (Wyoming, USA): Geology, v. 47, p. 1020–1024, https://doi.org/10.1130/G46419.1.

Henry, C.D., Hinz, N.H., Faulds, J.E., Colgan, J.P., John, D.A., Brooks, E.R., Cassel, E.J., Garside, L.J., Davis, D.A., and Castor, S.B., 2012, Eocene–Early Miocene paleotopography of the Sierra Nevada–Great Basin–Nevadaplano based on widespread ash-flow tuffs and paleovalleys: Geosphere, v. 8, p. 1–27, https://doi.org/10.1130/GES00727.1.

Honig, S., 2020, Early Eocene drainage evolution of the Idaho River, Green River Basin, Wyoming [M.S. thesis]: Madison, Wisconsin, University of Wisconsin-Madison, 75 p.

Hyland, E.G., and Sheldon, N.D., 2013, Coupled CO2-climate response during the Early Eocene Climatic Optimum: Palaeogeography, Palaeoclimatology, Palaeoecology, v. 369, p. 125–135, https://doi.org/10.1016/j.palaeo.2012.10.011.

Ingersoll, R.V., Bullard, T.F., Ford, R.L., Grimm, J.P., Pickle, J.D., and Sares, S.W., 1984, The effect of grain size on detrital modes: A test of the Gazzi-Dickinson point-counting method: Journal of Sedimentary Petrology, v. 54, p. 103–116.

Inglis, G.N., et al., 2020, Global mean surface temperature and climate sensitivity of the early Eocene Climatic Optimum (EECO), Paleocene–Eocene Thermal Maximum (PETM), and latest Paleocene: Climate of the Past, v. 16, p. 1953–1968, https://doi.org/10.5194/cp-16-1953-2020.

Jagniecki, E.A., and Lowenstein, T.K., 2015, Evaporites of the Green River Formation, Bridger and Piceance Creek Basins: Deposition, diagenesis, paleobrine chemistry, and Eocene atmospheric CO2, in Smith, M.E., and Carroll, A.R., eds., Stratigraphy and Paleolimnology of the Green River Formation, Western USA: Dordrecht, Netherlands, Springer, p. 277–312, https://doi.org/10.1007/978-94-017-9906-5_11.

Jolliffe, I.T., and Cadima, J., 2016, Principal component analysis: A review and recent developments: Philosophical Transactions of the Royal Society A: Mathematical, Physical and Engineering Sciences, v. 374, https://doi.org/10.1098/rsta.2015.0202.

King, C., 1878, Report of the Geological Exploration of the Fortieth Parallel Report, Volume 1: Systematic Geology: Professional Paper 18 of the Engineer Department, U.S. Army, 803 p.

Krueger, R., 2017, Fluvial response to warming during the early Eocene climatic optimum, Green River Basin, Wyoming [M.Sc. thesis]: Flagstaff, Arizona, Northern Arizona University, 91 p.

Lauretano, V., Zachos, J.C., and Lourens, L.J., 2018, Orbitally paced carbon and deep-sea temperature changes at the peak of the early Eocene climatic optimum: Paleoceanography and Paleoclimatology, v. 33, p. 1050–1065, https://doi.org/10.1029/2018PA003422.

Leary, R.J., et al., 2020, Provenance of Pennsylvanian-Permian sedimentary rocks associated with the Ancestral Rocky Mountains orogeny in southwestern Laurentia: Implications for continental-scale Laurentian sediment transport systems: Lithosphere, v. 12, p. 88–121, https://doi.org/10.1130/L1115.1.

Liu, S., Nummedal, D., Yin, P., and Luo, H., 2005, Linkage of Sevier thrusting episodes and late Cretaceous foreland basin megasequences across southern Wyoming (USA): Basin Research, v. 17, p. 487–506, https://doi.org/10.1111/j.1365-2117.2005.00277.x.

Love, J.D., 1970, Cenozoic geology of the Granite Mountains area, Central Wyoming: U.S. Geological Survey Professional Paper 495-C, 154 p., https://doi.org/10.3133/pp495C.

Lowenstein, T.K., Jagniecki, E.A., Carroll, A.R., Smith, M.E., Renaut, R.W., and Owen, R.B., 2017, The Green River salt mystery: What was the source of the hyperalkaline lake waters?: Earth-Science Reviews, v. 173, p. 295–306, https://doi.org/10.1016/j.earscirev.2017.07.014.

Machlus, M.L., Ramezani, J., Bowring, S.A., Hemming, S.R., Tsukui, K., and Clyde, W.C., 2015, A strategy for cross-calibrating U-Pb chronology and astrochronology of sedimentary sequences: An example from the Green River Formation, Wyoming, USA: Earth and Planetary Science Letters, v. 413, p. 70–78, https://doi.org/10.1016/j.epsl.2014.12.009.

Mott, L.V., and Drever, J.I., 1983, Origin of uraniferous phosphatic beds in Wilkins Peak Member of Green River Formation, Wyoming: AAPG Bulletin, v. 67, p. 70–82.

Odom, I.E., Doe, T.W., and Dott, R.H., 1976, Nature of feldspar-grain size relations in some quartz-rich sandstones: Journal of Sedimentary Research, v. 46, p. 862–870.

Oriel, S.S., and Tracey, J., 1970, Uppermost Cretaceous and Tertiary stratigraphy of Fossil Basin, southwestern Wyoming: U.S. Geological Survey Professional Paper 635, 53 p., https://doi.org/10.3133/pp635.

Parrish, E.C., Carroll, A.R., Gregorich, H., Smith, M.E., and Schwaderer, C., 2023, Watershed-scale provenance heterogeneity within Eocene nonmarine basin fill: Southern Greater Green River Basin, western USA: Geological Society of America Bulletin, https://doi.org/10.1130/B36822.1.

Payros, A., Ortiz, S., Millán, I., Arostegi, J., Orue-Etxebarria, X., and Apellaniz, E., 2015, Early Eocene climatic optimum: Environmental impact on the North Iberian continental margin: Geological Society of America Bulletin, v. 127, p. 1632–1644, https://doi.org/10.1130/B31278.1.

Pietras, J.T., and Carroll, A.R., 2006, High-resolution stratigraphy of an underfilled lake basin: Wilkins Peak Member, Eocene Green River Formation, Wyoming, U.S.A.:

Journal of Sedimentary Research, v. 76, p. 1197–1214, https://doi.org/10.2110/jsr.2006.096.

Pietras, J.T., Carroll, A.R., and Rhodes, M.K., 2003, Lake basin response to tectonic drainage diversion: Eocene Green River Formation, Wyoming: Journal of Paleolimnology, v. 30, p. 115–125, https://doi.org/10.1023/A:1025518015341.

Pipiringos, G.N., 1955, Tertiary rocks in the central part of the Great Divide Basin, Sweetwater County, Wyoming: Wyoming Geological Association Guidebook, 10th Annual Field Conference, p. 100–104.

Powell, J.W., 1876, Report of the geology of the eastern portion of the Uinta Mountains and region of country adjacent thereto, *in* U.S. Geological and Geographical Survey of the Territories, Second Division: Washington, D.C., U.S. Government Print Office, p. 1–209, https://doi.org/10.3133/70039913.

Roehler, H.W., 1992, Correlation, composition, areal distribution, and thickness of Eocene stratigraphic units, greater Green River basin, Wyoming, Utah, and Colorado: U.S. Geological Survey Professional Paper 1506-E, 49 p., https://doi.org/10.3133/pp1506E.

Roehler, H.W., 1993, Eocene climates, depositional environments, and geography, Greater Green River Basin, Wyoming, Utah, and Colorado: U.S. Geological Survey Professional Paper 1506-F, 74 p., https://doi.org/10.3133/pp1506F.

Romans, B.W., Castelltort, S., Covault, J.A., Fildani, A., and Walsh, J.P., 2016, Environmental signal propagation in sedimentary systems across timescales: Earth-Science Reviews, v. 153, p. 7–29, https://doi.org/10.1016/j.earscirev.2015.07.012.

Schwaderer, C.W., 2022, Discrimination of primary versus recycled detrital zircon provenance signals in the late Laramide foreland, Western U.S. [M.Sc. thesis]: Madison, Wisconsin, University of Wisconsin–Madison, 130 p.

Sewall, J.O., and Sloan, L.C., 2006, Come a little bit closer: A high-resolution climate study of the early Paleogene Laramide foreland: Geology, v. 34, p. 81–84, https://doi.org/10.1130/G22177.1.

Sharman, G.R., Covault, J.A., Stockli, D.F., Wroblewski, A.F.J., and Bush, M.A., 2017, Early Cenozoic drainage reorganization of the United States Western Interior—Gulf of Mexico sediment routing system: Geology, v. 45, p. 187–190, https://doi.org/10.1130/G38765.1.

Smith, M.E., Carroll, A.R., and Singer, B.S., 2008a, Synoptic reconstruction of a major ancient lake system: Eocene Green River Formation, western United States: Geological Society of America Bulletin, v. 120, p. 54–84, https://doi.org/10.1130/B26073.1.

Smith, M.E., Carroll, A.R., and Mueller, E.R., 2008b, Elevated weathering rates in the Rocky Mountains during the Early Eocene Climatic Optimum: Nature Geoscience, v. 1, p. 370–374, https://doi.org/10.1038/ngeo205.

Smith, M.E., Chamberlain, K.R., Singer, B.S., and Carroll, A.R., 2010, Eocene clocks agree: Coeval ^{40}Ar/^{39}Ar, U-Pb, and astronomical ages from the Green River Formation: Geology, v. 38, p. 527–530, https://doi.org/10.1130/G30630.1.

Smith, M.E., Carroll, A.R., Scott, J.J., and Singer, B.S., 2014a, Early Eocene carbon isotope excursions and landscape destabilization at eccentricity minima: Green River Formation of Wyoming: Earth and Planetary Science Letters, v. 403, https://doi.org/10.1016/j.epsl.2014.06.024.

Smith, M.E., Carroll, A.R., Jicha, B.R., Cassel, E.J., and Scott, J.J., 2014b, Paleogeographic record of Eocene Farallon slab rollback beneath western North America: Geology, v. 42, p. 1039–1042, https://doi.org/10.1130/G36025.1.

Smith, M.E., Carroll, A.R., and Scott, J.J., 2015, Stratigraphic expression of climate, tectonism, and geomorphic forcing in an underfilled lake basin: Wilkins Peak Member of the Green River Formation, *in* Smith, M.E., and Carroll, A.R., eds., Stratigraphy and Paleolimnology of the Eocene Green River Formation, Western U.S.: Dordrecht, Netherlands, Springer, p. 61–102, https://doi.org/10.1007/978-94-017-9906-5_4.

Smith, M.E., Werner, S.H., Buscombe, D., Finnegan, N.J., Sumner, E.J., and Mueller, E.R., 2018, Seeking the shore: Evidence for active submarine canyon head incision due to coarse sediment supply and focusing of wave energy: Geophysical Research Letters, v. 45, p. 12,403–12,413, https://doi.org/10.1029/2018GL080396.

Smoot, J.P., 1983, Depositional subenvironments in an arid closed basin; the Wilkins Peak Member of the Green River Formation (Eocene), Wyoming, U.S.A.: Sedimentology, v. 30, p. 801–827, https://doi.org/10.1111/j.1365-3091.1983.tb00712.x.

Somarin, A., 2015, Chemostratigraphy and identification of fine-grained sedimentary rocks using portable XRF: Gulf Coast Association of Geological Societies Transactions, v. 65, p. 355–360.

Sullivan, R., 1985, Origin of lacustrine rocks of the Wilkins Peak Member, Wyoming: AAPG Bulletin, v. 69, p. 13–35.

Tofte, M., and Carroll, A., 2022, Spatiotemporal quantification of organic matter accumulation in the Eocene Green River Formation, Bridger Basin, Wyoming: Utah Geological Association Publication, v. 50, p. 1–20, https://doi.org/10.31711/ugap.v50i.117.

Valeton, I., 1994, Element concentration and formation of ore deposits by weathering: Catena, v. 21, p. 99–129, https://doi.org/10.1016/0341-8162(94)90006-X.

Walters, A.P., Carroll, A.R., Meyers, S.R., and Lowenstein, T.K., 2023, Influence of lake-basin morphology on climate-sediment transfer functions: Early Eocene Wilkins Peak Member, Green River Formation, Wyoming: Geological Society of America Bulletin, v. 135, p. 2664–2677, https://doi.org/10.1130/B36566.1.

Yonkee, W.A., and Weil, A.B., 2015, Tectonic evolution of the Sevier and Laramide belts within the North American Cordillera orogenic system: Earth-Science Reviews, v. 150, p. 531–593, https://doi.org/10.1016/j.earscirev.2015.08.001.

Zachos, J., Pagani, M., Sloan, L., Thomas, E., and Billups, K., 2001, Trends, Global Rhythms, Aberrations in Global Climate 65 Ma to Present: Science, v. 292, p. 686–693, https://doi.org/10.1126/science.1059412.

Zachos, J.C., Dickens, G.R., and Zeebe, R.E., 2008, An early Cenozoic perspective on greenhouse warming and carbon-cycle dynamics: Nature, v. 451, p. 279–283, https://doi.org/10.1038/nature06588.

Zonneveld, J.-P., Bartels, W.S., and Clyde, W.C., 2003, Stratal architecture of an early Eocene fluvial-lacustrine depositional system, Little Muddy Creek area, Southwestern Green River Basin, Wyoming, *in* Raynolds, R.G., and Flores, R.M., eds., Cenozoic Systems of the Rocky Mountain Region: Rocky Mountain Section, SEPM (Society for Sedimentary Geology), p. 253–287.

Zuffa, G.G., 1980, Hybrid arenites: Their composition and classification: Journal of Sedimentary Petrology, v. 50, p. 21–29.